Tight-binding model for the electronic properties of simple hexagonal graphite

J.-C. Charlier and J.-P. Michenaud
Laboratoire de Physico-Chimie et de Physique des Matériaux, Université Catholique de Louvain, 1 place Croix du Sud, B-1348 Louvain-La-Neuve, Belgium

X. Gonze
Clark Hall, Cornell University, Ithaca, New York 14853

J.-P. Vigneron
Institute for Studies in Interface Sciences (ISIS), Facultés Universitaires Notre-Dame de la Paix, 61 rue de Bruxelles, B-5000 Namur, Belgium

(Received 31 May 1991; revised manuscript received 26 August 1991)

The band structure of graphite with the hypothetical simple hexagonal structure has been investigated near the Fermi energy, using a *tight-binding* approximation. Some general features of the structure of the π bands in the neighborhood of the zone edge are obtained and are expressed in terms of appropriate parameters. The Fermi surface is analyzed. The density of states and the resulting behavior near the Fermi level are compared to the results obtained for the Bernal structure (Slonczewski-Weiss-McClure model) and for the rhombohedral structure (Haering-McClure model). Possible application to disordered graphite (turbostratic) is also discussed.

I. INTRODUCTION

Graphite has been studied for many years.[1] Most of these studies deal with the Bernal structure,[2] whereas the layers of hexagonally arranged carbon atoms are alternately stacked ($ABAB$ stacking). Natural (and synthesized) graphite contains varying amounts of rhombohedral modifications of graphite, where the layers are stacked in an $ABCABC$ fashion.

Since the 1980s, renewed interest in understanding the physics of graphite has resulted from work on the class of physically and technologically important materials called graphite intercalation compounds (GIC's).[3] In these materials, various superlattices are produced by insertion of atoms or molecules either between each pair of neighboring carbon layers n and $(n+1)$ (nth-stage intercalation). The physical properties of these materials vary drastically with the stage of intercalation and with the intercalating species. For instance, intercalation with alkaline metals increases the conductivity of graphite from semimetallic behavior up to levels comparable to the noble metals. In the GIC's, the carbon layers can be stacked in different ways, either similar to the Bernal structure or with layers of carbon atoms located directly on top of each other (AAA stacking). Such is the case for the different stages of Li intercalated graphite (LiC_n). The hypothetical configuration where the carbon atoms in consecutive layers are directly above each other has not been identified in pure graphite.

Our comparative theoretical study of three modifications of graphite (hypothetical AAA stacking, Bernal, and rhombohedral) is a first step for the qualitative understanding of the electronic properties of the turbostratic graphite, which is another modification of graphite without any periodicity in the z direction (perpendicular to the planes of hexagonally arranged carbon atoms)[4] but can also stimulate future experimental work relative to the electronic properties of graphite intercalation compounds.

A comparison of their theoretical band structures will be presented in this study. We expect the three band structures to be nearly identical because they are all dominated by the two-dimensional in-plane interactions. A two-dimensional calculation is indeed sufficient to explain the main features of the energy bands of graphite[5] except for the region close to the Fermi energy (ε_F). This region, which determines the electronic properties but also the material response function to low-energy excitations, such as cyclotron resonance and infrared absorption, is exactly where the three structures differ significantly from each other. To find these important differences in the π bands close to the Fermi energy (region dominating transport properties), we have to adapt the Slonczewski-Weiss-McClure[5] model, valid for Bernal graphite, to our hypothetical configuration: the graphite stacking AAA. This will be the aim of the next section. The model of the rhombohedral graphite has already been established by Haering[6] and by McClure as a modification of the Slonczewski-Weiss-McClure model.

An *ab initio* study of the electronic energies of Bernal graphite, around the Fermi level, has already been done: the obtained results are very close to experiment.[7] We plan a similar study of simple hexagonal graphite, for which the present model is an important component.

II. THEORETICAL BAND STRUCTURE OF SIMPLE HEXAGONAL GRAPHITE

The band structure of the hypothetical configuration of the stacking AAA is now investigated using the nearest-neighbor *tight-binding* approximation. This calculation is

 ©1991 The American Physical Society

based on the $2p_z$ orbitals, as was done by Wallace[8] for the Bernal structure. More detailed investigations of the Bernal structure[9] have shown that the result of Wallace for *two-dimensional graphite* are unaffected by a more general treatment. However, for the three-dimensional structure, a more general treatment admits the possibility of "vertical" overlap of the π bands (along $K-H$), while in the Wallace treatment these bands touch, but do not overlap (i.e., 2D graphite is a zero-band-gap semiconductor). The mistake originates from the nearest-neighbor approximation: the effect of interaction between nearest-neighboring planes must be included. In the Wallace approximation, the vertical edges of the Brillouin zone are lines of constant energy, a condition not required by the crystal symmetry. A variation of energy along these edges results in the vertical overlap mentioned above. So, in addition to the two-dimensional-type behavior, it is necessary to find the dependence of energy on the component of the wave vector parallel to the c axis (k_z).

The crystal structure of simple hexagonal graphite is shown in Fig. 1(a). In this structure, the carbon atoms within a single layer of graphite form a plane hexagonal lattice (assumed to be the xy plane), in which the atoms are separated by the a distance. The layers are then placed on top of each other in a sequence which we may denote A-A-A-A..., indicating that all the planes have the same projection on the xy plane. The interlayer distance is labeled by the c distance and the unit cell contains two carbon atoms. The unit cell and the chosen primitive lattice vectors are shown in Fig. 2.

In the *tight-binding* approximation, the interactions between wave functions centered on neighboring atoms are parametrized and generate the Hamiltonian to be diagonalized. A 2D model is a first approximation for graphite: in-plane interactions are included.

Each carbon atom possesses four valence electrons. The $2s$ electrons have a spherical symmetry wave function, $\psi_{2s}(\mathbf{r})$, and the $2p$ electrons have the following wave functions: $\psi_{2p}^{(x)}(\mathbf{r})$, $\psi_{2p}^{(y)}(\mathbf{r})$, and $\psi_{2p}^{(z)}(\mathbf{r})=\varphi(\mathbf{r})$. ψ_{2s}, $\psi_{2p}^{(x)}$, and $\psi_{2}^{(y)}$ form three tight bindings with the three neighboring atoms of the plane (hybridized orbitals σ; cf. Fig. 3).

The fourth wave function $\psi_{2p}^{(z)}$ will generate π orbitals. It is an antisymmetrical wave function which is not hybridized in the 2D model, as shown in Fig. 3.

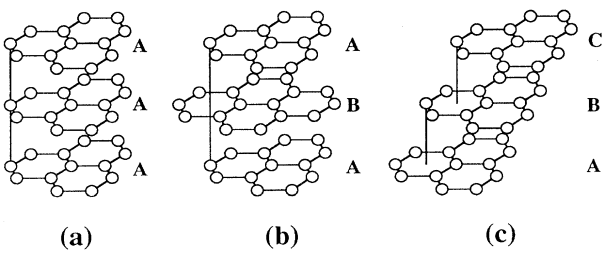

FIG. 1. Comparison of the usual three crystalline structures of graphite which differ one from each other by the shift imposed to the graphitic planes in the stacking: (a) *AAAAAA*, simple hexagonal graphite; (b) *ABABAB*, hexagonal graphite (Bernal structure); (c) *ABCABC*, rhombohedral graphite.

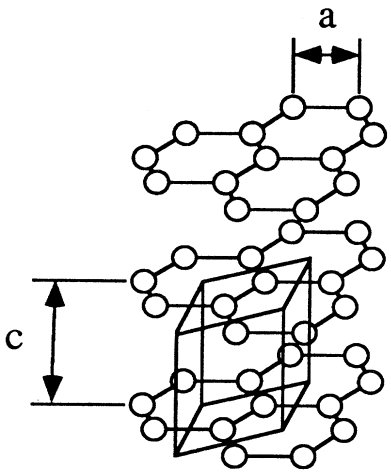

FIG. 2. Unit cell of the simple hexagonal graphite (solid line). a is the distance between two nearest neighbors while c is the interlayer distance. The dimensions of the unit cell are $2*a*\cos[30°]$ and c.

The 2D model is a reasonable first approximation for graphite because the π-electronic orbitals overlap weakly when interplane interactions are taken into account.

In studies of Bernal graphite,[5,9] it was shown that the separation between the π band and the σ band is large enough to neglect the influence of the σ electrons on the band structure near the Fermi energy. In the following, we restrict ourselves to the π-derived band structure.

Using the atomic π orbitals, it is possible to construct the Bloch functions:

$$\psi_{\mathbf{k}}^{A}(\mathbf{r})=\frac{1}{\sqrt{N}}\sum_{A}\varphi(\mathbf{r}-\mathbf{r}_A)\exp(i\mathbf{k}\cdot\mathbf{r}_A)\ , \tag{1}$$

$$\psi_{\mathbf{k}}^{A'}(\mathbf{r})=\frac{1}{\sqrt{N}}\sum_{A'}\varphi(\mathbf{r}-\mathbf{r}_{A'})\exp(i\mathbf{k}\cdot\mathbf{r}_{A'})\ . \tag{2}$$

The summation is extended to all the atoms of the crystal. A' are the first-neighboring atoms of A. These atoms are called B in the Bernal structure because their chemical environment in this structure is different from the one of A atoms. For AAA stacking, A and A'

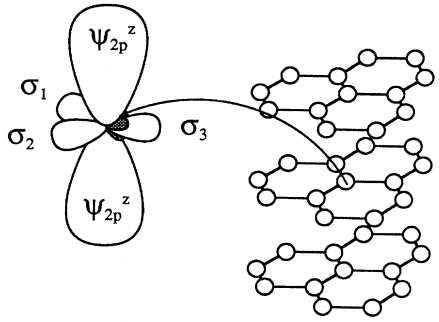

FIG. 3. Representation of the carbon valence orbitals: the three hybridized σ orbitals and $\psi_{2p}^{(z)}$, the nonhybridized π orbital.

atoms have the same chemical environment. The positions of the atoms A and A' are designed by the corresponding vectors $\mathbf{r}_A$ and $\mathbf{r}_{A'}$. The number of cells in the crystal is N.

In our *tight-binding* approximation, we neglect the overlapping integrals:

$$\int \varphi(\mathbf{r}-\mathbf{r}_{A_i}\pm n\mathbf{c})\varphi(\mathbf{r}-\mathbf{r}_{A_j}\pm m\mathbf{c})d\tau=\delta_{ij}\delta_{nm} \tag{3}$$

with

$$\mathbf{r}_{A_i},\mathbf{r}_{A_j}=\mathbf{r}_A \text{ or } \mathbf{r}_{A'} \text{ and } n,m=0,1,2,3\ldots$$

and where $\mathbf{c}$ is the unit-cell basal vector of range c along the $\mathbf{k}_z$ direction.

The wave functions $\Psi(\mathbf{r})$ are linear combinations of the two Bloch functions:

$$\Psi(\mathbf{r})=\lambda\psi_{\mathbf{k}}^{A}(\mathbf{r})+\lambda'\psi_{\mathbf{k}}^{A'}(\mathbf{r}) . \tag{4}$$

So, defining

$$\Lambda=\begin{bmatrix}\lambda\\ \lambda'\end{bmatrix} \tag{5}$$

the eigenvalues equation becomes

$$\begin{bmatrix}\langle\psi_{\mathbf{k}}^{A}|H|\psi_{\mathbf{k}}^{A}\rangle & \langle\psi_{\mathbf{k}}^{A}|H|\psi_{\mathbf{k}}^{A'}\rangle\\ \langle\psi_{\mathbf{k}}^{A'}|H|\psi_{\mathbf{k}}^{A}\rangle & \langle\psi_{\mathbf{k}}^{A'}|H|\psi_{\mathbf{k}}^{A'}\rangle\end{bmatrix}\Lambda = E\begin{bmatrix}\langle\psi_{\mathbf{k}}^{A}|\psi_{\mathbf{k}}^{A}\rangle & \langle\psi_{\mathbf{k}}^{A}|\psi_{\mathbf{k}}^{A'}\rangle\\ \langle\psi_{\mathbf{k}}^{A'}|\psi_{\mathbf{k}}^{A}\rangle & \langle\psi_{\mathbf{k}}^{A'}|\psi_{\mathbf{k}}^{A'}\rangle\end{bmatrix}\Lambda . \tag{6}$$

At the Fermi level, the π-band structure of the simple hexagonal graphite, which is calculated in this study with a *tight-binding* approximation, can be described by a model of five parameters: $E_0,\alpha_0,\alpha_1,\alpha_2,\alpha_3$. These parameters, which define the interaction energies between π orbitals from different carbon atoms inside the plane or from plane to plane, are defined in the following expressions:

$$E_0=\int \varphi(\mathbf{r}-\mathbf{r}_A)H\varphi(\mathbf{r}-\mathbf{r}_A)d\tau , \tag{7}$$

where E_0 is the energy of the nonhybridized π orbitals in the crystal,

$$\alpha_0=\int \varphi(\mathbf{r}-\mathbf{r}_A)H\varphi(\mathbf{r}-\mathbf{r}_A-\mathbf{b}_l)d\tau , \tag{8}$$

where the $\mathbf{b}_l$ vectors connect an atom to its nearest neighbors in the graphitic plane ($l=1,2,3$).

The α_0 parameter represents the interaction between first-neighboring atoms in a graphitic monolayer,

$$\alpha_1=\int \varphi(\mathbf{r}-\mathbf{r}_A\pm\mathbf{c})H\varphi(\mathbf{r}-\mathbf{r}_A)d\tau . \tag{9}$$

The α_1 parameter is related to the interaction between two atoms of the same projection on the xy plane, from two neighboring graphitic planes,

$$\alpha_2=\int \varphi(\mathbf{r}-\mathbf{r}_A\pm 2\mathbf{c})H\varphi(\mathbf{r}-\mathbf{r}_A)d\tau . \tag{10}$$

The α_2 parameter represents the interaction between two atoms of the same projection on the xy plane, from two next-neighboring graphitic planes,

$$\alpha_3=\int \varphi(\mathbf{r}-\mathbf{r}_A)H\varphi(\mathbf{r}-\mathbf{r}_A-\mathbf{b}_l\pm\mathbf{c})d\tau . \tag{11}$$

The α_3 parameter represents the interaction between two first-neighboring atoms of different projections on the xy plane, from two neighboring graphitic planes. These α_i parameters are presented in Fig. 4.

In Appendix A, we establish the expression for the Hamiltonian:

$$\begin{bmatrix}E_0+\alpha_1\Gamma+\alpha_2(\Gamma^2-2) & f(k_x;k_y)(\alpha_0+\alpha_3\Gamma)\\ f^*(k_x;k_y)(\alpha_0+\alpha_3\Gamma) & E_0+\alpha_1\Gamma+\alpha_2(\Gamma^2-2)\end{bmatrix}\Lambda=E\Lambda , \tag{12}$$

where

$$f(k_x;k_y)=\sum_{l=1}^{3}\exp(i\mathbf{k}\cdot\mathbf{b}_l) . \tag{13}$$

The solution of the eigenvalues problem Eq. (12) is

$$E_{\pm}=E_0+\alpha_1\Gamma+2\alpha_2\left[\frac{\Gamma^2}{2}-1\right]\pm(\alpha_0+\alpha_3\Gamma)|f(k_x;k_y)| , \tag{14}$$

where $\Gamma=2\cos(\mathbf{k}_z\cdot\mathbf{c})$ as in the SWMcC model:

$$\frac{\Gamma^2}{2}-1=\cos(2\mathbf{k}_z\cdot\mathbf{c}) \tag{15}$$

and

$$|f(k_x;k_y)|=\left[1+4\cos^2\left[k_y\frac{a}{2}\right]+4\cos\left[k_y\frac{a}{2}\right]\cos\left[k_x\frac{\sqrt{3}a}{2}\right]\right]^{1/2} . \tag{16}$$

In the following section, we study the solution Eq. (14) near the *HKH* edge of the Brillouin zone, where the overlap appears.

III. BAND STRUCTURE NEAR AN EDGE OF THE BRILLOUIN ZONE

The perturbations due to the interactions between graphitic planes introduce weak modifications to the 2D model, which described graphite as a zero-band-gap semiconductor. A small overlap is induced and the Fermi surface remains located near the edge *HKH* of the Brillouin zone[10] (cf. Fig. 5).

In the neighborhood of this edge, the energy will be calculated by a -$\mathbf{k}\cdot\mathbf{p}$- perturbation expansion.

Let us define $\mathbf{k}_0$ as the vector which starts at the centre of the Brillouin zone and reaches the edge *HKH*:

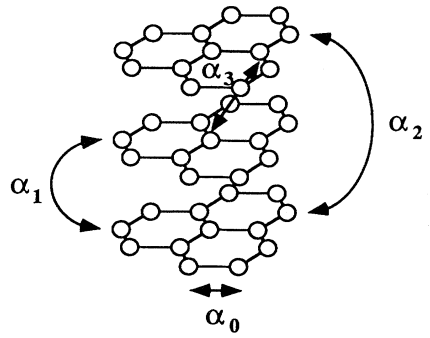

FIG. 4. Correspondence (arrows) between the parameters α_i of this model and the interaction between the individual atoms in the simple hexagonal graphite lattice.

$$\mathbf{k}_0=\mathbf{k}_{\Gamma K} \ . \tag{17}$$

In the particular case of the edge *HKH*, the scalar product $\mathbf{k}_0\cdot\mathbf{b}_l$ equals, respectively, $0,2\pi/3,4\pi/3$ for $l=1,2,3$.

Suppose now that we are slightly away from this edge:

$$\mathbf{k}=\mathbf{k}_0+\mathbf{x} \ . \tag{18}$$

Expressed in cylindrical coordinates,

$$\mathbf{x}=\mathbf{x}(x,\theta) \ , \tag{19}$$

where $x=|\mathbf{x}|$ and θ is the angle between $(0,k_y,0)$ and $\mathbf{x}$ (cf. Fig. 6).

In that particular case, the evaluation of the function $f(k_x;k_y)$ is

$$f(k_x;k_y)=\sum_{l=1}^{3}\exp(i\mathbf{k}_0\cdot\mathbf{b}_l)\exp(i\mathbf{x}\cdot\mathbf{b}_l) \tag{20}$$

$$=\sum_{l=1}^{3}\exp(i\mathbf{k}_0\cdot\mathbf{b}_l)[1+i\mathbf{x}\cdot\mathbf{b}_l-\tfrac{1}{2}(\mathbf{x}\cdot\mathbf{b}_l)^2+\cdots] \ . \tag{21}$$

The first term of the Taylor development gives no contribution because

$$\sum_{l=1}^{3}\exp(i\mathbf{k}_0\cdot\mathbf{b}_l)=0 \ . \tag{22}$$

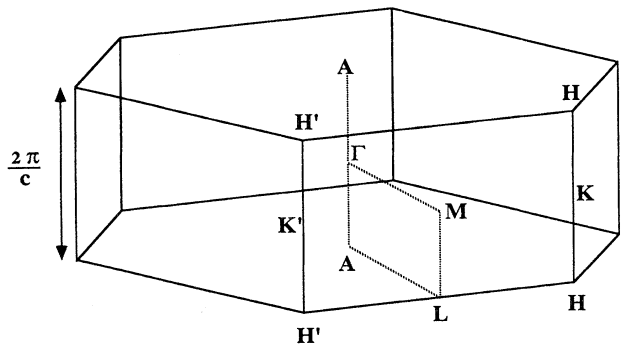

FIG. 5. Brillouin zone of the simple hexagonal graphite, showing several high-symmetry points. Each symmetric point is labeled with the usual Bouckaert-Smoluchowski-Wigner (Ref. 10) notation (Γ, *A*,*H*,*K*,*L*,*M*).

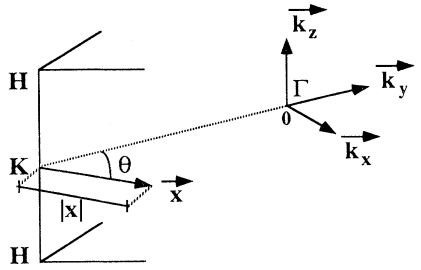

FIG. 6. Orientation of the axis in the reciprocal space. x is the distance away from the edge *HKH* and θ is the angle between this vector and the Γ-*K* direction.

We will take into account the two following terms of the Taylor development:

$$f(k_x;k_y)\cong\frac{\sqrt{3}}{2}a|\mathbf{x}|\exp(i\theta)+\frac{a^2}{8}|\mathbf{x}|^2\exp(-i2\theta) \ . \tag{23}$$

So, the absolute value of the function $f(k_x;k_y)$ present in the energy expression is

$$|f(k_x;k_y)|=\left[\frac{3a^2}{4}|\mathbf{x}|^2+\frac{\sqrt{3}a^3}{16}|\mathbf{x}|^3\cos(3\theta)+\frac{a^4}{64}|\mathbf{x}|^4\right]^{1/2} . \tag{24}$$

The effect of the term in $|\mathbf{x}|^2$ in the Taylor development Eq. (23) is to break the cylindrical symmetry, leading to a trigonal symmetry [$\cos(3\theta)$]. The simulation of this influence on the symmetry has been represented in Fig. 7. The maximum effect of this term is on the order of 5%. It will be neglected in the following. It could

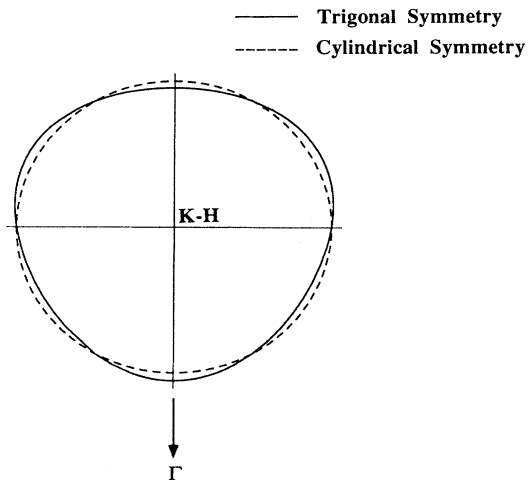

FIG. 7. Trigonal symmetry, around the edge *HKH*, introduced by the $|x^2|$ term in the Taylor development Eq. (23). The dashed line represents the cylindrical symmetry while the solid line shows the breaking of this symmetry into a trigonal symmetry (in arbitrary units). As can be seen on this figure, the influence of this term is weak.

then be considered that there is no more dependence on θ: the Fermi surface possesses a cylindrical symmetry around the edge *HKH*. This is in contrast with the Bernal structure of graphite: retaining only the first term in the corresponding Taylor expansion will not lead to a cylindrical symmetry. The trigonal warping of the Fermi surface of the Bernal graphite is well known and described by the γ_3 parameter of the SWMcC model.

The absolute value of the function $f(k_x;k_y)$ is then reduced to its first term:

$$|f(k_x;k_y)|=\frac{\sqrt{3}a}{2}|\mathbf{x}|=S \ . \tag{25}$$

The energy around the edge *HKH* is

$$E_{\pm}=E_0+\alpha_1\Gamma+2\alpha_2\left[\frac{\Gamma^2}{2}-1\right]\pm S(\alpha_0+\alpha_3\Gamma) \ . \tag{26}$$

Along the vertical edge of the Brillouin zone, $S=(\sqrt{3}/2)a|\mathbf{x}|=0$.

There is a twofold degeneracy (the spin degeneracy is not taken into account) of the energy bands along the *HK* band edge (cf. Fig. 8):

$$E_{\pm}=E_0+\alpha_1\Gamma+\alpha_2(\Gamma^2-2) \ . \tag{27}$$

At the *K* point, the energy reduces to

$$E_K=E_0+2\alpha_1+2\alpha_2 \ . \tag{28}$$

At the *H* point, the energy reduces to

$$E_H=E_0-2\alpha_1+2\alpha_2 \ . \tag{29}$$

The difference in these energies is simply related to the α_1 parameter of the model

$$E_K-E_H=4\alpha_1 \ , \tag{30}$$

and the energy, at the middle of the *H* and *K* points, gives a relation between two other parameters: E_0 and α_2.

$$E_{KH/2}=E_0-2\alpha_2 \ , \tag{31}$$

In the neighborhood of the vertical edge of the Brillouin zone,

$$S=\frac{\sqrt{3}}{2}a|\mathbf{x}|\neq 0 \ .$$

There is a lift of degeneracy of the energy $E_{\pm}$ between the *H* point and the *K* point. In the particular case where $x\neq 0$, the wave functions correspond to two different eigenvalues for the same Schrödinger equation.

In a plane perpendicular to the hexagonal axis, that contains the *K* point (cf. Fig. 9), the energies equal

$$E_{K\pm}=E_0+2\alpha_1+2\alpha_2\pm S(\alpha_0+2\alpha_3) \ . \tag{32}$$

In a plane perpendicular to the hexagonal axis, that contains the *H* point (cf. Fig. 10), the energies equal

$$E_{H\pm}=E_0-2\alpha_1+2\alpha_2\pm S(\alpha_0-2\alpha_3) \ . \tag{33}$$

This dispersion around the *HKH* edge introduces a weak overlap in the neighborhood of this Brillouin zone corner (cf. Fig. 11).

The Fermi energy E_F will be close to E_0, but slightly different if either α_2 or α_3 are nonzero. Holes will be transferred from the neighborhood of *H* to the neighborhood of the *K* point. An electron pocket appears near *H* and a hole pocket near *K*.

The energy, as a function of k_z and the polar coordinates centered on the edge *HKH* of the Brillouin zone, is

$$E=E_0+2\alpha_1\cos(\mathbf{k}_z\cdot\mathbf{c})+2\alpha_2\cos(2\mathbf{k}_z\cdot\mathbf{c}) \pm\frac{\sqrt{3}}{2}ax[\alpha_0+2\alpha_3\cos(\mathbf{k}_z\cdot\mathbf{c})] \ . \tag{34}$$

The lower sign corresponds to the valence band, and the upper sign corresponds to the conduction band. The lines of constant energy in a plane perpendicular to the *c* axis are circles. The Fermi surface possesses a cylindrical symmetry as shown in Fig. 12. As mentioned before, the trigonal warping due to the term in $|x|^2$ in the Taylor development of the -**k**·**p**- perturbation expansion has not been taken into account in this representation.

Due to the hexagonal symmetry of the lattice, one Fermi surface is centered on each of the six vertical edges of the Brillouin zone. Each Fermi surface is composed of a main pocket of holes, centered at the *K* point, which is

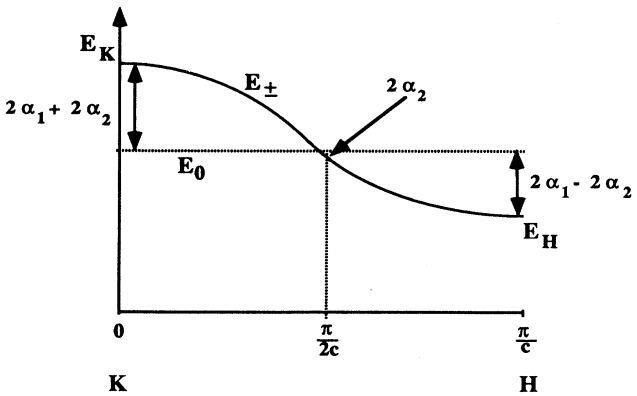

FIG. 8. Band structure around the Fermi level along the *HKH* edge of the Brillouin zone (in arbitrary units). There is a degeneracy of the two energy bands along this direction.

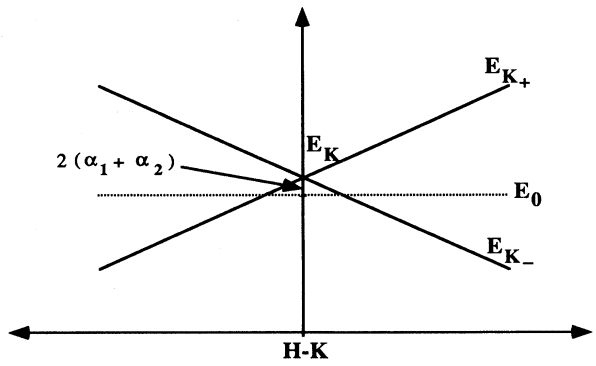

FIG. 9. Linear dispersion relations at the *K* point, in the neighborhood of the edge *HKH* of the Brillouin zone (in arbitrary units).

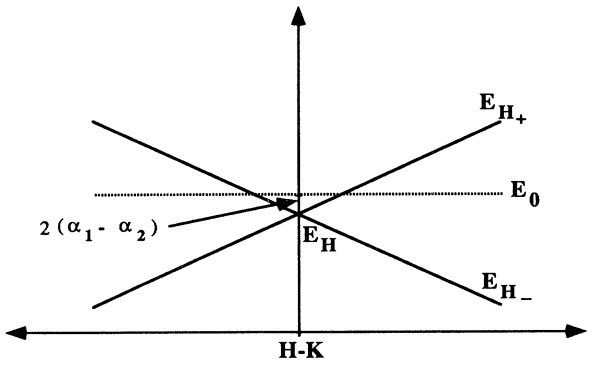

FIG. 10. Linear dispersion relations at the H point, in the neighborhood of the edge HKH of the Brillouin zone (in arbitrary units).

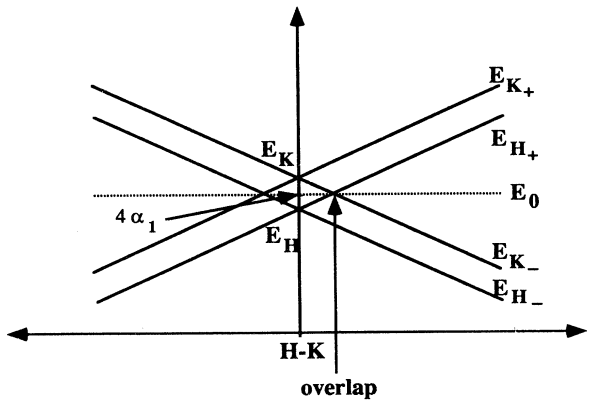

FIG. 11. Weak overlap between conduction (E_{K-}) and valence (E_{H+}) bands near the Fermi level away from the edge HKH of the Brillouin zone (in arbitrary units).

surrounded by two smaller pockets of electrons centered at the two H points. The simple hexagonal graphite has no minority carriers as the hexagonal graphite (SWMcC: minority holes).

In contrast to the case of the Bernal graphite, it is possible to get an analytical expression for the different volumes of the various pockets of electrons and holes of the different Fermi surfaces. On an edge of the Brillouin zone, the limits of the hole pocket are $(-k_z^*;k_z^*)$ while those of the electron pockets are $(-\pi/c;-k_z^*)$ and $(k_z^*;\pi/c)$, where k_z^* is the solution of $E_F=E_\pm$, where $E_\pm$ is given by Eq. (27).

$$k_z^*=+\frac{1}{c}\arccos\left[\frac{-\alpha_1\pm\sqrt{\alpha_1^2+4\alpha_2(E_F-E_0+2\alpha_2)}}{4\alpha_2}\right]. \tag{35}$$

From revolution-volume formulas, the hole volume is

$$V_{\text{hole}}(E_F)=2\pi\int_{\max\{-2;\Gamma^*\}}^{2}\left[\frac{E_F-E_0-\alpha_1\Gamma-\alpha_2(\Gamma^2-2)}{\frac{\sqrt{3}a}{2}(\alpha_0+\alpha_3\Gamma)}\right]^2\frac{1}{c\sqrt{4-\Gamma^2}}d\Gamma\ , \tag{36}$$

where

$$\Gamma^*=\frac{-\alpha_1+\sqrt{\alpha_1^2+4\alpha_2(E_F-E_0+2\alpha_2)}}{2\alpha_2}\ .$$

A similar expression can respectively be found for the electron volume.

Analytical integration of Eq. (36) is possible and has been established using the MATHEMATICA™ package. However, the resulting expressions are cumbersome and of little help.

Plausible numerical values for α_0 and α_3 give $\alpha_3/\alpha_0\approx 0.01$ (see Sec. IV). This latter fact, combined with $-2<\Gamma<2$, allows the following approximation:

$$(\alpha_0+\alpha_3\Gamma)^{-1}=\alpha_0^{-1}\left[1-\frac{\alpha_3}{\alpha_0}\Gamma\right]+O((\alpha_3/\alpha_0)^2)\ ,$$

which induces an error on the order of 2.0×10^{-4}. In this approximation, the analytical expressions for electron and hole volumes are less cumbersome and can be found in Appendix B.

The analytical relation, established by equating the numbers of holes and the numbers of electrons, appears to involve transcendental functions of the variables in an essentially nonalgebraic way. An analytical expression for the Fermi energy is then impossible but a numerical approximation has been established for the plausible set of parameters (see Sec. IV): ($\alpha_0=3.2$ eV; $\alpha_1=0.4$ eV; $\alpha_2,\alpha_3=0.04$ eV).

$$E_F=E_0+0.013\,063\,635\,43\ \text{eV}\ . \tag{37}$$

As mentioned before, the Fermi energy E_F will be close to E_0, but slightly different if either α_2 or α_3 are nonzero. When both parameters are zero, the Fermi energy is reduced to E_0.

The density of states can be calculated using the following formula:

$$N(E)=\frac{d}{dE}V_{\text{electron}}(E)-\frac{d}{dE}V_{\text{hole}}(E)\ . \tag{38}$$

The analytical expression of the density of states can also be found in Appendix B. Figure 13 represents the total density of electronic states $[N(E)=N_e(E)+N_h(E)]$ of the simple hexagonal graphite. Outside the region $-2\alpha_1+2\alpha_2<E<2\alpha_1+2\alpha_2$, the density of states is the same as the two-dimensional density of states. The total density of states for a "hypothetical" pure material is more or less 19×10^{-3} $\text{eV}^{-1}\,\text{atom}^{-1}$ compared with

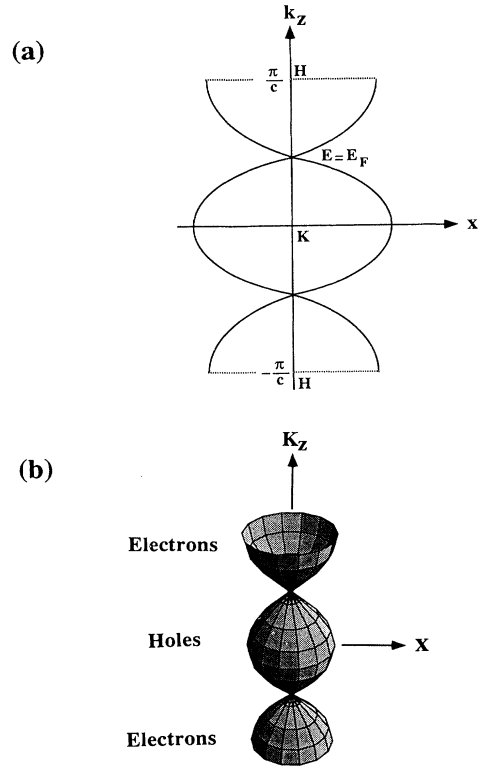

FIG. 12. Fermi surface of the simple hexagonal graphite which is composed of a pocket of electrons centered at the K point and two half pockets of holes centered at the H point. (a) Intersection between the Fermi surface and the ΓHK plane (in arbitrary units). (b) 3D Fermi surface (in arbitrary units).

about 5.5×10^{-3} eV^{-1} atom^{-1} for hexagonal graphite for our set of plausible values for the α_i parameters. The simple hexagonal graphite is a "semimetal" whose overlap of the order of 1.6 eV ($=4\alpha_1$) is much greater than the overlaps of the two other graphitic semimetals. The comparison between the densities of states and the band

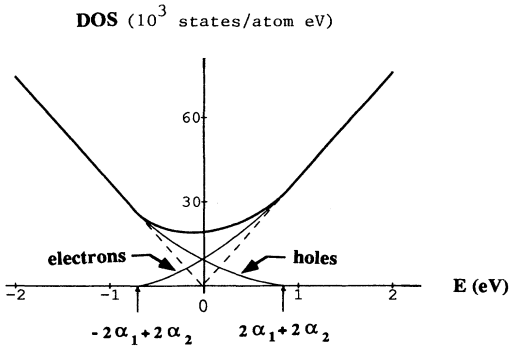

FIG. 13. The density of electronic states in simple hexagonal graphite, calculated under the assumption that $\alpha_0=3.2$ eV; $\alpha_1=0.04$ eV; $\alpha_2,\alpha_3=0.04$ eV (in number of states per atom eV). The heavy line is the total density of states, and the partial densities of states for holes and electrons are indicated. The dashed line gives the density of states for the two-dimensional model.

structures, near the Fermi level, of the different modifications of graphite will be the aim of the next section.

IV. COMPARISON OF THE ENERGIES AROUND THE FERMI LEVEL AND THE DENSITIES OF STATES OF THE DIFFERENT STRUCTURES

As the three band structures of the different stackings are nearly identical except near the Fermi level,[11] Fig. 14 compares in details the region close to the Fermi energy for the different modifications. The AAA stacking exposed in this study is compared to the Slonczewski-Weiss-McClure model for the Bernal structure and also to the Haering-McClure model for the rhombohedral graphite.

To be comparable, in each case, the unfolded bands are presented between K and H (corresponding to the smallest possible unit cell for each of the structures) and H^* (common zone).

For the $ABAB$ stacking [Fig. 14(a)], we reproduce the well-known three bands (ε_1, ε_2, and ε_3 at the K point) of the SWMcC model,[5] where the π orbitals are totally localized on atoms which have a neighbor in the first-neighboring graphitic plane (A atoms). These eigenvalues of the SWMcC Hamiltonian[5] are given by the roots of the following equation:

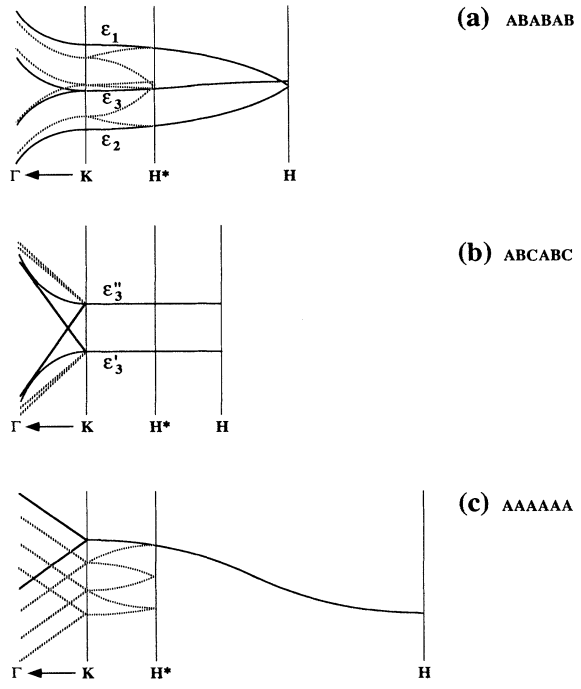

FIG. 14. Details of the band structure in the vicinity of the Fermi level for the three modifications of graphite presented in Fig. 1. The bands that arise due to multiple foldings along the k_z direction are shown by dashed lines. The H^* point corresponds to the common zone while the H point is associated with the smallest possible unit cell for each of the structures.

$$(\varepsilon_1-\varepsilon)(\varepsilon_2-\varepsilon)(\varepsilon_3-\varepsilon)^2$$

$$-\frac{\hbar^2k^2p^2}{m^2}[(\varepsilon_1-\varepsilon)(\varepsilon_3-\varepsilon)(1+\nu)^2+(\varepsilon_2-\varepsilon)(\varepsilon_3-\varepsilon)(1-\nu)^2+4\frac{\gamma_3^2}{\gamma_0^2}\cos^2(\mathbf{k}_z\cdot\mathbf{c}/2)(\varepsilon_1-\varepsilon)(\varepsilon_1-\varepsilon)]$$

$$-2\frac{\hbar^3k^3p^3}{m^3}\frac{\gamma_3}{\gamma_0}\cos(\mathbf{k}_z\cdot\mathbf{c}/2)\cos(3\theta)[(\varepsilon_1-\varepsilon)(1+\nu)^2-(\varepsilon_2-\varepsilon)(1-\nu)^2]+\left[\frac{\hbar kp}{m}\right]^4(1+\nu)^2(1-\nu)^2=0\ , \tag{39}$$

where $\nu=2(\gamma_4/\gamma_0)\cos(\mathbf{k}_z\cdot\mathbf{c}/2)$ and $p=\frac{1}{2}\sqrt{3}(m/\hbar)\gamma_0 a$.

Along each vertical axis of the Brillouin zone (HKH), the eigenvalues are

$$\varepsilon_1=\Delta+\gamma_1\Gamma+\tfrac{1}{2}\gamma_5\Gamma^2\ , \tag{40}$$

$$\varepsilon_2=\Delta-\gamma_1\Gamma+\tfrac{1}{2}\gamma_5\Gamma^2\ , \tag{41}$$

$$\varepsilon_3=\tfrac{1}{2}\gamma_2\Gamma^2\ , \tag{42}$$

where Γ, in this case, is defined as $2\cos(\mathbf{k}_z\cdot\mathbf{c}/2)$.

These three states are totally different; ε_1 is an antibonding state whereas ε_2 is a bonding one. The ε_3 state is degenerate and localized on atoms which do not have any neighbors in the first-neighboring graphite plane (B atoms). The degeneracy of the two ε_3 levels is lifted as we move away from the zone edge, and this is indicated on the left-hand side of Fig. 14(a).

The splitting of the antibonding and bonding states (ε_1 and ε_2) of p_z orbitals gradually decreases approaching the H point. At the H point, due to the phase reversal, bonding and antibonding states are degenerate. This degeneracy is maintained throughout the plane KAL.

For the $ABCABC$ stacking [Fig. 14(b)], we reproduce the two nearly dispersionless bands (ε_3' and ε_3'' at the K point) coming from the Haering-McClure model.[6] Along each vertical edge of the Brillouin zone, these two eigenvalues are

$$\left.\begin{matrix}\varepsilon_3''\\ \varepsilon_3'\end{matrix}\right\}=E_0\pm A\cos(3\mathbf{k}_z\cdot\mathbf{c})\ , \tag{43}$$

where $A=(2\gamma_1/\gamma_0)(b\gamma_1'+\gamma_2'')$ and $b=\gamma_2'/\gamma_1+\gamma_1'/\gamma_0$. ($\gamma_1'\approx\gamma_3$ or γ_4; $\gamma_2',\gamma_2''\approx\gamma_2$).

Along the HKH edge, there is still an energy gap between these two bands. However, there are some points in the Brillouin zone where the gap is zero; such points are very close to the edge of the hexagonal zone.

In the unfolded case, each of these bands is triply degenerate. The main difference between these two first structures is that no atoms in the rhombohedral structure form a continuous chain perpendicular to the graphitic planes throughout the entire crystal as in the Bernal structure. These nearly dispersionless bands are then the counterparts of the ε_3 band in the $ABAB$ structure. It is also clear that the Fermi level does not cross the bands between K and H (unlike the $ABAB$ case), but inside the Brillouin zone, very close to the HKH zone edge.[6] The rhombohedral graphite is also a "semimetal," but with a very weak overlap.

For the AAA stacking [Fig. 14(c)], we can immediately see that bands similar to ε_1 and ε_2 in Fig. 14(a) are present in Fig. 14(c), while no flat bands like ε_3 are present. This is understandable since all the atoms in the AAA structure have a neighbor in the first-neighboring graphitic plane. Consequently, each band in the folded structure is doubly degenerate. The energies along the vertical edge of the Brillouin zone are expressed by Eq. (27).

The comparison between our parameters α_0, α_1, α_2, α_3 and the well-known seven SWMcC parameters γ_i is very relevant. It will allow us to have first-approximation values for the AAA-model parameters.

The α_0 parameter which represents the interaction between first-neighboring atoms in a graphitic monolayer is equivalent to the γ_0 parameter of the SWMcC model. In both cases, the parameter can be calculated in a 2D monolayer ($\gamma_0=3.2$ eV).

The α_1 parameter which is related to the interaction between two atoms of same projection on the xy plane from two neighboring graphitic planes is related to the γ_1 parameter of the SWMcC model. In both models, this parameter established the width of the π bands at the K point (folded region) of the Brillouin zone, which is equal, respectively, to $4\alpha_1$ or $2\gamma_1$ ($\gamma_1\approx0.4$ eV).

The α_2 parameter, which represents the interaction between two atoms of the same projection on the xy plane from two next-neighboring graphitic planes, must also be of the same order of magnitude as the γ_5 parameter of the SWMcC model ($\gamma_5\approx0.04$ eV).

The α_3 parameter, which represents the interaction between two first-neighboring atoms of different projections on the xy plane from two neighboring graphitic planes, is related to the γ_4 parameter of the SWMcC model ($\gamma_4\approx0.04$ eV).

We will use the value quoted for the γ_i parameters as a first approximation for the α_i parameters.

The total densities of electronic states [$N(E)=N_e(E)+N_h(E)$] of the different modifications of graphite are calculated and compared in Fig. 15.

Outside the region $-2\gamma_1<E<2\gamma_1$, the density of states of the hexagonal graphite [Fig. 15(a)] is similar to the two-dimensional graphite density of states. This semimetal possesses an overlap of the order of 40 meV ($=2\gamma_2$). The total density of states for pure material is more or less 5.5×10^{-3} eV^{-1} atom^{-1}.

Outside the region $-A<E<A$, the density of states

of the rhombohedral graphite [Fig. 15(b)] is similar to the two-dimensional graphite density of states. This semimetal possesses an overlap of the order of 20 meV ($=2A$). The total density of states for pure material is more or less $0.25\times10^{-3}\,\mathrm{eV}^{-1}\,\mathrm{atom}^{-1}$. Around the Fermi level, the nearly dispersionless bands of the Haering-McClure model (ε_3' and ε_3'' at the K point) possess an artificial 2D character producing discontinuities in the DOS.

Outside the region $-2\alpha_1+2\alpha_2<E<2\alpha_1+2\alpha_2$, the density of states of the simple hexagonal graphite [Fig. 15(c)] is similar to the two-dimensional graphite density of states. This semimetal possesses an overlap of the order of 1.6 eV ($=4\alpha_1$). The total density of states for pure material is more or less $19\times10^{-3}\,\mathrm{eV}^{-1}\,\mathrm{atom}^{-1}$ for our set of plausible values for the α_i parameters. The simple hexagonal graphite is a semimetal whose overlap and density of states are greater than the ones of the two other semimetals presented before.

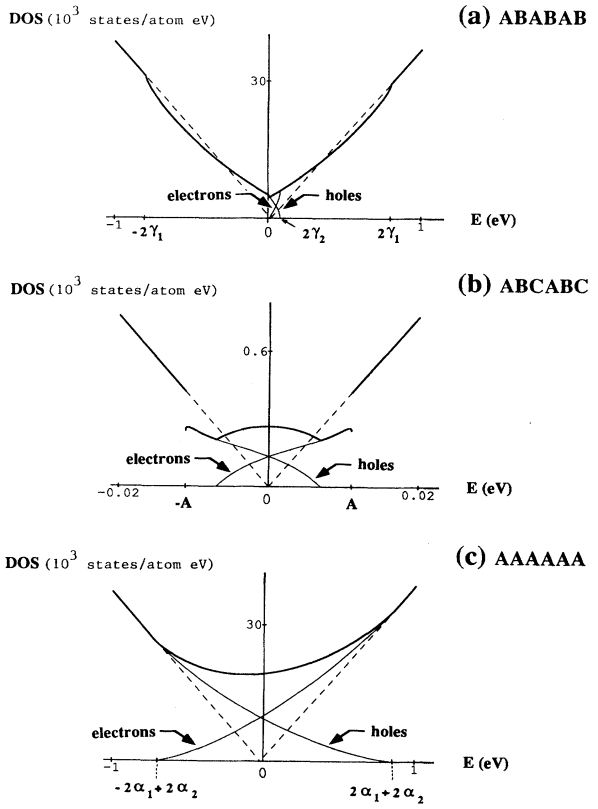

FIG. 15. Details of the densities of states for the three modifications of graphite presented in Fig. 1 [(a) *ABABAB*; (b) *ABCABC*; (c) *AAAAAA*]. These densities of states are calculated under the assumption that $\alpha_0,\gamma_0=3.2$ eV; $\alpha_1,\gamma_1=0.4$ eV; $\gamma_2=-0.02$ eV; $\gamma_3=0.3$ eV; $\alpha_2,\alpha_3,\gamma_4,\gamma_5=0.04$ eV (in number of states per atom eV). The heavy line is the total density of states, and the partial densities of states for holes and electrons are indicated. The dashed line gives the density of states for the two-dimensional model. The density of states of the rhombohedral graphite is detailed in an interval 50 times weaker than the two others.

By the same technique used for the *ab initio* study of the electronic energies of graphite around the Fermi level,[7] we plan to study the numerical values of the α_i parameters of the simple-hexagonal-graphite model, present their variations with the interlayer distance $|c|$ (deformation potentials) and compare them with the other models for the different modifications of graphite. The optimal value of the c distance, calculated self-consistently, will also be provided.

V. DISCUSSION

The commonly used model established for dilute GIC's (Ref. 3) shows that the Fermi energy cuts the weakly dispersive band ε_3 similarly to the Slonczewski-Weiss model[5] for pure graphite. In the particular case of a dilute donor GIC, the increase of E_F leads to the production of a larger electron pocket and vanishing hole pockets. This model is very relevant for particular GIC's with *ABAB* stacking, like KC_n. However, for other GIC's with *AAA* stacking, like LiC_n, we can immediately see [cf. Fig. 14(c)] that the ε_3 band giving rise to the extremal orbits is absent for the *AAA* stacking. Consequently, the commonly used model for discussing the extremal orbits is irrelevant for dilute GIC's with carbon layer in *AAA* stacking.[11]

The turbostratic graphite is a particular stacking of parallel graphitic monolayers with no periodicity along the c axis and also with possible rotations of the different planes around the c axis. The irregularities of such a crystalline structure must lead to a "fuzzyness" of the lower and upper positions of the band structure: a distribution of the energy levels is more accurate than a definite relation between the energy and the wave vector. So, it seems reasonable to establish the electronic properties of the turbostratic graphite by superposition of some models corresponding to different crystalline structures. Some models are present in the literature: the Mrozowski model,[12] alteration of the Slonczewski-Weiss model,[13] the Deficiar turbostratic graphite model,[14] the turbostratic carbon model,[15] the simple two bands model,[16] and the bidimensional GaS model.[17] All these models try to explain the electronic properties of pregraphitic carbon with a preexisting model (like the SWMcC model). It would be interesting to study the turbostratic graphite by a combination of the three models compared in this study.

In conclusion, we have shown that various graphite modifications possess different electronic structure near E_F due to the different interlayer stacking order. Thus, in spite of the fact that graphite is predominantly a two-dimensional material, the weak interlayer interaction plays an important role in determining the π-electron structure near the E_F, the region dominating transport and low-energy excitation properties.

ACKNOWLEDGMENTS

We thank V. Bayot, G. Dresselhaus, Ph. Lambin, and L. Piraux for their interests in this work. We are also

grateful to M. S. Dresselhaus for a critical reading of the manuscript. One of the authors (J.-C.C.) has benefited from the financial support of the National Fund for Scientific Research (Belgium). This paper presents research results of the Belgian Program on Interuniversity Attraction Poles initiated by the Belgian State Prime Minister's Office-Science Policy Programming.

APPENDIX A

Development of the different matrix elements of the Hamiltonian:

$$\text{(i)}\quad \langle \psi_{\mathbf{k}}^{A}|H|\psi_{\mathbf{k}}^{A}\rangle = \int \psi_{\mathbf{k}}^{A*}(\mathbf{r})H\psi_{\mathbf{k}}^{A}(\mathbf{r})d\tau\ , \tag{A1}$$

$$= \frac{1}{N}\sum_{A_i}\sum_{A_j}\exp[i\mathbf{k}(\mathbf{r}_{A_i}-\mathbf{r}_{A_j})] \times \int \varphi(\mathbf{r}-\mathbf{r}_{A_j})H\varphi(\mathbf{r}-\mathbf{r}_{A_i})d\tau\ . \tag{A2}$$

If the study is limited to the two first-neighboring planes interactions, the precedent matrix element becomes

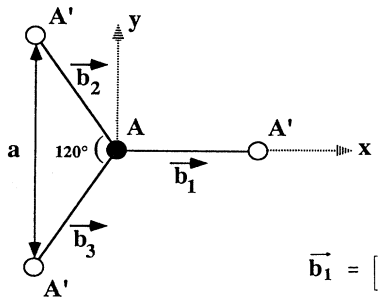

$$\vec{b_1} = \left[\frac{a}{\sqrt{3}}\ ;\ 0\right]$$

$$\vec{b_2} = \left[-\frac{a}{2\sqrt{3}}\ ;\ \frac{a}{2}\right]$$

$$\vec{b_3} = \left[-\frac{a}{2\sqrt{3}}\ ;\ -\frac{a}{2}\right]$$

FIG. 16. Representation of the in-plane first neighbors (A') of an A atom. The coordinates of the $\mathbf{b}_l$ vectors which connect an atom to its nearest neighbors are also presented in the xy plane.

$$\langle \psi_{\mathbf{k}}^{A}|H|\psi_{\mathbf{k}}^{A}\rangle \approx \frac{1}{N}\sum_{A}\left[\int \varphi(\mathbf{r}-\mathbf{r}_A)H\varphi(\mathbf{r}-\mathbf{r}_A)d\tau + \Gamma\int \varphi(\mathbf{r}-\mathbf{r}_A\pm\mathbf{c})H\varphi(\mathbf{r}-\mathbf{r}_A)d\tau + (\Gamma^2-2)\int \varphi(\mathbf{r}-\mathbf{r}_A\pm 2\mathbf{c})H\varphi(\mathbf{r}-\mathbf{r}_A)d\tau\right], \tag{A3}$$

where $\Gamma = 2\cos[\mathbf{k}_z^0\mathbf{c}]$.

$$\text{(ii)}\quad \langle \psi_{\mathbf{k}}^{A'}|H|\psi_{\mathbf{k}}^{A'}\rangle = \langle \psi_{\mathbf{k}}^{A}|H|\psi_{\mathbf{k}}^{A}\rangle\ , \tag{A4}$$

$$\text{(iii)}\quad \langle \psi_{\mathbf{k}}^{A}|H|\psi_{\mathbf{k}}^{A'}\rangle = \int \psi_{\mathbf{k}}^{A*}(\mathbf{r})H\psi_{\mathbf{k}}^{A'}(\mathbf{r})d\tau \tag{A5}$$

$$= \frac{1}{N}\sum_{A_i}\sum_{A_j'}\exp[i\mathbf{k}(\mathbf{r}_{A_j'}-\mathbf{r}_{A_i})] \times \int \varphi(\mathbf{r}-\mathbf{r}_{A_i})H\varphi(\mathbf{r}-\mathbf{r}_{A_j'})d\tau\ . \tag{A6}$$

In this study, the summation expressed in Eq. (13) is reduced to a summation on the three in-plane first-nearest neighbors and on the six first-nearest neighbors of the two first-neighboring graphitic planes of the A_i considered atom.

$\mathbf{r}_{A_j}$ is the vector which starts on A and finishes on one of its in-plane first neighbor.

$$\Longrightarrow \mathbf{r}_{A_j} = \mathbf{r}_{A_i} + \mathbf{b}_l\ , \tag{A7}$$

where $l = 1,2,3$.

Figure 16 represents the in-plane first neighbors of the A atom. In addition, the exponential inside the summation can be reduced to a function of $\mathbf{k}_x$ and $\mathbf{k}_y$.

$$\sum_{l=1}^{3}\exp(i\mathbf{k}_0\mathbf{b}_l) = \exp\left[i\mathbf{k}_x\frac{a}{\sqrt{3}}\right] + \exp\left[-i\mathbf{k}_x\frac{a}{2\sqrt{3}}\right]\exp\left[i\mathbf{k}_y\frac{a}{2}\right] + \exp\left[-i\mathbf{k}_x\frac{a}{2\sqrt{3}}\right]\exp\left[-i\mathbf{k}_y\frac{a}{2}\right]$$

$$= \exp\left[i\mathbf{k}_x\frac{a}{\sqrt{3}}\right] + 2\cos\left[\mathbf{k}_y\frac{a}{2}\right]\exp\left[-i\mathbf{k}_x\frac{a}{2\sqrt{3}}\right]$$

$$= f(\mathbf{k}_x;\mathbf{k}_y)\ , \tag{A8}$$

$$\sum_{l=1}^{3}\exp(i\mathbf{k}_0\mathbf{b}_l)\exp(\pm i\mathbf{k}_0\mathbf{c}) = f(\mathbf{k}_x;\mathbf{k}_y)[2\cos(\mathbf{k}_{z_0}\mathbf{c})]\ . \tag{A9}$$

The matrix element becomes

$$\langle \psi_{\mathbf{k}}^{A}|H|\psi_{\mathbf{k}}^{A'}\rangle \approx \frac{1}{N}\sum_{A}\left[f(\mathbf{k}_x;\mathbf{k}_y)\int \varphi(\mathbf{r}-\mathbf{r}_A)H\varphi(\mathbf{r}-\mathbf{r}_A-\mathbf{b}_l)d\tau + f(\mathbf{k}_x;\mathbf{k}_y)\Gamma\int \varphi(\mathbf{r}-\mathbf{r}_A)H\varphi(\mathbf{r}-\mathbf{r}_A-\mathbf{b}_l\pm\mathbf{c})d\tau\right] . \tag{A10}$$

(iv) $$\langle \psi_{\mathbf{k}}^{A'}|H|\psi_{\mathbf{k}}^{A}\rangle = \langle \psi_{\mathbf{k}}^{A}|H|\psi_{\mathbf{k}}^{A'}\rangle^{*} . \tag{A11}$$

APPENDIX B

Defining E_0 as the energetical reference, the analytical expressions for the electron and hole volumes are expressed in the different intervals of energy.

If $E < -2\alpha_1+2\alpha_2$, then there is no more electron pocket:

$$V_{\text{electron}}(E)=0 , \tag{B1}$$

$$V_{\text{hole}}(E)=\frac{8\pi}{3ca^2\alpha_0^2}\left[2\pi\left[\alpha_1^2+\alpha_2^2+\frac{E^2}{2}-\frac{4\alpha_1\alpha_3}{\alpha_0}(\alpha_2-E)+\frac{\alpha_3^2}{\alpha_0^2}(3\alpha_1^2+2\alpha_2^2-2\alpha_2E+E^2)\right]\right] . \tag{B2}$$

If $-2\alpha_1+2\alpha_2 < E < 2\alpha_1+2\alpha_2$, then

$$\begin{aligned}V_{\text{electron}}(E)=\frac{8\pi}{3ca^2\alpha_0^2}\Bigg[&\pi\left[\alpha_1^2+\alpha_2^2+\frac{E^2}{2}-\frac{4\alpha_1\alpha_3}{\alpha_0}(E+\alpha_2)+\frac{\alpha_3^2}{\alpha_0^2}(3\alpha_1^2+2\alpha_2^2+2\alpha_2E+E^2)\right]\\
&+\sqrt{4-\Gamma^{*2}}\Bigg\{2\alpha_1(E+2\alpha_2)+\frac{2\alpha_3}{\alpha_0}\left(\tfrac{52}{15}\alpha_2^2-4\alpha_1^2-8\alpha_2E-E^2\right)+\frac{8\alpha_1\alpha_3^2}{\alpha_0^2}\left[E+\frac{2\alpha_2}{15}\right]\\
&+\Gamma^{*}\left[\frac{\alpha_1^2}{2}-\frac{\alpha_2^2}{2}-\alpha_2E-\frac{2\alpha_1\alpha_3}{\alpha_0}(E+\alpha_2)+\frac{\alpha_3^2}{\alpha_0^2}\left[\frac{3\alpha_1^2}{2}+\alpha_2^2+\alpha_2E+\frac{E^2}{2}\right]\right]\\
&+\Gamma^{*2}\frac{32\alpha_2\alpha_3}{15\alpha_0}\left[\frac{\alpha_1\alpha_3}{\alpha_0}-\alpha_2\right]+\Gamma^{*3}\left[\frac{\alpha_2^2}{4}-\frac{\alpha_1\alpha_2\alpha_3}{\alpha_0}+\frac{\alpha_3^2}{2\alpha_0^2}\left[\frac{\alpha_1^2}{2}-\frac{\alpha_2^2}{3}+\alpha_2E\right]\right]\\
&+\Gamma^{*4}\frac{2\alpha_2\alpha_3}{5\alpha_0}\left[\frac{\alpha_1\alpha_3}{\alpha_0}-\alpha_2\right]+\Gamma^{*5}\frac{\alpha_2^2\alpha_3^2}{6\alpha_0^2}\Bigg\}\\
&+(4-\Gamma^{*2})^{3/2}\left[-\tfrac{2}{3}\alpha_1\alpha_2+\frac{2\alpha_3}{3\alpha_0}(\alpha_1^2-4\alpha_2^2+2\alpha_2E)+\frac{2\alpha_1\alpha_3^2}{\alpha_0^2}\left[\frac{2\alpha_2}{3}-E\right]\right]\\
&-\arcsin(\Gamma^{*}/2)\left[2\alpha_1^2+2\alpha_2^2+E^2-\frac{8\alpha_1\alpha_3}{\alpha_0}(E+\alpha_2)+\frac{2\alpha_3^2}{\alpha_0^2}(3\alpha_1^2+2\alpha_2^2+2\alpha_2E+E^2)\right]\Bigg] ,\end{aligned} \tag{B3}$$

$$V_{\text{hole}}(E)=V_{\text{electron}}(-E) . \tag{B4}$$

If $E > 2\alpha_1+2\alpha_2$, then there is no more hole pocket:

$$V_{\text{electron}}(E)=\frac{8\pi}{3ca^2\alpha_0^2}\left[2\pi\left[\alpha_1^2+\alpha_2^2+\frac{E^2}{2}-\frac{4\alpha_1\alpha_3}{\alpha_0}(E+\alpha_2)+\frac{\alpha_3^2}{\alpha_0^2}(3\alpha_1^2+2\alpha_2^2+2\alpha_2E+E^2)\right]\right] , \tag{B5}$$

$$V_{\text{hole}}(E)=0 . \tag{B6}$$

Resolving Eq. (38), we obtain the analytical expression for the density of states in the different intervals of energy:

If $E < -2\alpha_1+2\alpha_2$, then

$$N(E)=\frac{8\pi}{3ca^2\alpha_0^2}\left[2\pi\left[-E-\frac{4\alpha_1\alpha_3}{\alpha_0}+\frac{\alpha_3^2}{\alpha_0^2}(2\alpha_2-E)\right]\right] . \tag{B7}$$

If $-2\alpha_1+2\alpha_2 < E < 2\alpha_1+2\alpha_2$, then

$$
\begin{aligned}
N(E)=\frac{8\pi}{3ca^2\alpha_0^2}\Bigg[\frac{1}{\zeta\sqrt{4-\Gamma^{*2}}}\Bigg\{32\left[\frac{\alpha_1^2+(E^2/2)}{\alpha_2}+\alpha_2+\frac{4\alpha_1\alpha_3}{\alpha_0}-\frac{4\alpha_1\alpha_3 E}{\alpha_0\alpha_2}+\frac{\alpha_3^2(3\alpha_3^2+E^2)}{\alpha_0^2\alpha_2}+\frac{2\alpha_3^2(E+\alpha_2)}{\alpha_0^2}\right]\\
+8\Gamma^*\left[\alpha_1\left[1+\frac{E}{2\alpha_2}+\frac{\frac{4}{15}\alpha_3^2}{\alpha_0^2}\right]+\frac{\alpha_3(\frac{26}{15}\alpha_2-2E)}{\alpha_0}-\frac{\alpha_3}{\alpha_0\alpha_2}\left[2\alpha_1^2+\frac{E^2}{2}-\frac{2\alpha_1\alpha_3 E}{\alpha_0}\right]\right]\\
+\Gamma^{*2}\left[\frac{\alpha_1^2}{\alpha_2}+2E-\alpha_2-\frac{4\alpha_1\alpha_3}{\alpha_0}+\frac{2\alpha_3^2(E+\alpha_2)}{\alpha_0^2}-\frac{\alpha_3}{\alpha_0\alpha_2}\left[4\alpha_1 E-\frac{\alpha_3}{\alpha_0}(E+3\alpha_1^2)\right]\right]\\
+\Gamma^{*3}\frac{64\alpha_3}{15\alpha_0}\left[\frac{\alpha_1\alpha_3}{\alpha_0}-\alpha_2\right]+\Gamma^{*4}\left[\frac{\alpha_2}{2}-\frac{2\alpha_1\alpha_3}{\alpha_0}+\frac{\alpha_3^2}{\alpha_0^2}\left[E-\frac{\alpha_2}{3}+\frac{\alpha_1^2}{2\alpha_2}\right]\right]\\
+\Gamma^{*5}\frac{4\alpha_3}{5\alpha_0}\left[\frac{\alpha_1\alpha_3}{\alpha_0}-\alpha_2\right]+\Gamma^{*6}\frac{\alpha_2\alpha_3^2}{3\alpha_0^2}\Bigg\}\\
+\sqrt{4-\Gamma^{*2}}\Bigg\{4\alpha_1+\frac{\alpha_2-2E}{\zeta}-\frac{\alpha_1^2}{\alpha_2\zeta}+\frac{4\alpha_3}{\alpha_0}\left[\frac{\alpha_1}{\zeta}-2E-4\alpha_1\right]\\
+\frac{2\alpha_3^2}{\alpha_0^2}\left[8\alpha_1-\frac{\alpha_2+E}{\zeta}\right]+\frac{\alpha_3}{\alpha_0\alpha_2\zeta}\left[\frac{4\alpha_1E-3\alpha_1^2\alpha_3}{\alpha_0}-\frac{\alpha_3E^2}{\alpha_0}\right]\\
+\Gamma^*\left[2\alpha_2-\frac{4\alpha_1}{\zeta}+\frac{4\alpha_3}{\alpha_0}\left[\frac{2E}{\zeta}-\alpha_1-\frac{28\alpha_2}{15\zeta}\right]+\frac{2\alpha_3^2}{\alpha_0^2}\left[E+2\alpha_2-\frac{8\alpha_1}{15\zeta}\right]+\frac{4\alpha_1\alpha_3}{\alpha_2\alpha_0\zeta}\left[\alpha_1+E\frac{\alpha_3}{\alpha_0}\right]\right]\\
+\Gamma^{*2}\left[-\frac{3\alpha_2}{2\zeta}+\frac{6\alpha_1\alpha_3}{\alpha_0\zeta}+\frac{\alpha_3^2}{\alpha_0^2\zeta}\left[\alpha_2-3E-\frac{3\alpha_1^2}{2\alpha_2}\right]\right]\\
+\Gamma^{*3}\left[\frac{\alpha_2\alpha_3}{\alpha_0}\left[\alpha_3+\frac{16}{5\zeta}\right]-\frac{\alpha_3^2}{\alpha_0^2\zeta}\left[\frac{16\alpha_1}{5}+\frac{5\alpha_2}{3}\Gamma^*\right]\right]\Bigg\}\\
+(4-\Gamma^{*2})^{3/2}\left[\frac{8\alpha_2\alpha_3}{3\alpha_0}-\frac{4\alpha_1\alpha_3^2}{3\alpha_0^2}\right]+\arcsin(\Gamma^*/2)\left[\frac{16\alpha_1\alpha_3}{\alpha_0}-\frac{8\alpha_3^2(E+\alpha_2)}{\alpha_0^2}-4E\right]\Bigg], \qquad \text{(B8)}
\end{aligned}
$$

where

$$
\Gamma^*=\frac{-\alpha_1+\sqrt{\alpha_1^2-4\alpha_2(E_F-E_0-2\alpha_2)}}{2\alpha_2}=\frac{-\alpha_1}{2\alpha_2}+\frac{\zeta}{2}\ .
$$

If $E>2\alpha_1+2\alpha_2$, then

$$
N(E)=\frac{8\pi}{3ca^2\alpha_0^2}\left[2\pi\left[E-\frac{4\alpha_1\alpha_3}{\alpha_0}+\frac{\alpha_3^2}{\alpha_0^2}(2\alpha_2+E)\right]\right]. \qquad \text{(B9)}
$$

[1]For example, see references in M. S. Dresselhaus, G. Dresselhaus, K. Sugihara, I. L. Spain, and H. Goldberg, *Graphite Fibers and Filaments,* Springer Series in Materials Science Vol. 5 (Springer-Verlag, Berlin, 1988); N. B. Brandt, S. M. Chudinov, and Ya.G. Ponomarev, *Semimetals, Graphite and its Compounds,* Modern Problems in Condensed Matter Sciences Vol. 20.1 (North-Holland, Amsterdam, 1988); J.-C. Charlier, X. Gonze, and J.-P. Michenaud, Phys. Rev. B **43**, 4579 (1991).

[2]J. D. Bernal, Proc. R. Soc. London Ser. A **106**, 749 (1924).

[3]M. S. Dresselhaus, G. Dresselhaus, and J. E. Fischer, Phys. Rev. B **15**, 3180 (1977); J. E. Fischer and T. E. Thompson, Phys. Today **31** (1978); J. E. Fischer, Phys. Chem. Mater. Layered Struct. **5** (1978); N. A. W. Holzwarth, S. Rabii, and L. A. Girifalco, Phys. Rev. B **18**, 5190 (1978); N. A. W. Holzwarth, *ibid.* **21**, 3665 (1980); G. Dressehaus and S. Y. Leung, Solid State Commun. **35**, 819 (1980); M. Saint Jean and C. Rigaux, Rev. Chim. Min. **19**, 521 (1982).

[4]A. Marchand, in *Les Modèles Électroniques des Carbones,* edited by A. Pacault (Masson and Cie, Paris, 1965), Vol. 1, Pt. III, p. 232.

[5]J. C. Slonczewski and P. R. Weiss, Phys. Rev. **109**, 272 (1958); J. W. McClure, *ibid.* **108**, 612 (1957).

[6]R. R. Haering, Can. J. Phys. **36**, 352 (1958); J. W. McClure, Carbon **7**, 425 (1969).

[7]J.-C. Charlier, X. Gonze, and J.-P. Michenaud, Phys. Rev. B **43**, 4579 (1991).

[8]P. R. Wallace, Phys. Rev. **71**, 622 (1947).

[9]C. A. Coulson and R. Taylor, Proc. Phys. Soc. A **65**, 815 (1952); W. M. Lomer, Proc. R. Soc. London Ser. A **227**, 330

(1955); J. C. Slonczewski, Ph.D. thesis, Rutgers University (1955); J. C. Slonczewski and P. R. Weiss, Phys. Rev. **99**, 636 (1955); **109**, 272 (1958); D. F. Johnston, Proc. R. Soc. London Ser. A **227**, 349 (1955); **237**, 48 (1956); F. J. Corbato (unpublished); J. W. McClure, Phys. Rev. **108**, 612 (1957).

[10]L. P. Bouckaert, R. Smoluchowski, and E. Wigner, Phys. Rev. **50**, 58 (1936).

[11]L. Samuelson, I. P. Batra, and C. Roetti, Solid State Commun. **33**, 217 (1980).

[12]S. Mrozowski, Phys. Rev. **77**, 838 (1950); **85**, 609 (1952); **86**, 1056 (1952).

[13]P. Nozières, Phys. Rev. **109**, 1510 (1958).

[14]A. Marchand, Carbon **1**, 75 (1963).

[15]A. Marchand, Chem. Rev. **241**, 489 (1955).

[16]C. A. Klein, J. Appl. Phys. **33**, 3338 (1962).

[17]A. Pacault and A. Marchand, Chem. Rev. **241**, 489 (1955); A. Marchand, Ann. Chim. **13**, 2 (1957); **13**, 469 (1957).